SANDIA REPORT

SAND2014-20188
Unlimited Release
Printed December 2014

Fundamental Aspects of Selective Melting Additive Manufacturing Processes

Frank B. van Swol and James E. Miller

Prepared by
Sandia National Laboratories
Albuquerque, New Mexico 87185 and Livermore, California 94550

Sandia National Laboratories is a multi-program laboratory managed and operated by Sandia Corporation, a wholly owned subsidiary of Lockheed Martin Corporation, for the U.S. Department of Energy's National Nuclear Security Administration under contract DE-AC04-94AL85000.

Sandia National Laboratories

Issued by Sandia National Laboratories, operated for the United States Department of Energy by Sandia Corporation.

Available to DOE and DOE contractors from
U.S. Department of Energy
Office of Scientific and Technical Information
P.O. Box 62
Oak Ridge, TN 37831

Telephone: (865) 576-8401
Facsimile: (865) 576-5728
E-Mail: reports@adonis.osti.gov
Online ordering: http://www.osti.gov/bridge

Available to the public from
U.S. Department of Commerce
National Technical Information Service
5285 Port Royal Rd
Springfield, VA 22161

Telephone: (800) 553-6847
Facsimile: (703) 605-6900
E-Mail: orders@ntis.fedworld.gov
Online ordering: http://www.ntis.gov/help/ordermethods.asp?loc=7-4-0#online

SAND2014-20188
Unlimited Release
Printed December 2014

Fundamental Aspects of Selective Melting Additive Manufacturing Processes

Frank B. van Swol
Department 1814
Sandia National Laboratories
Albuquerque, NM 87185-1411
fbvansw@sandia.gov

James E. Miller
Department 1815
Sandia National Laboratories
Albuquerque, NM 87185-1349
jemille@sandia.gov

Abstract

Certain details of the additive manufacturing process known as selective laser melting (SLM) affect the performance of the final metal part. To unleash the full potential of SLM it is crucial that the process engineer in the field receives guidance about how to select values for a multitude of process variables employed in the building process. These include, for example, the type of powder (e.g., size distribution, shape, type of alloy), orientation of the build axis, the beam scan rate, the beam power density, the scan pattern and scan rate. The science-based selection of these settings constitutes an intrinsically challenging multi-physics problem involving heating and melting a metal alloy, reactive, dynamic wetting followed by re-solidification. In addition, inherent to the process is its considerable variability that stems from the powder packing. Each time a limited number of powder particles are placed, the stacking is intrinsically different from the previous, possessing a different geometry, and having a different set of contact areas with the surrounding particles. As a result, even if all other process parameters (scan rate, etc) are exactly the same, the shape and contact geometry and area of the final melt pool will be unique to that particular configuration. This report identifies the most important issues facing SLM, discusses the fundamental physics associated with it and points out how modeling can support the additive manufacturing efforts.

Acknowledgment

Thanks to Amy Sun for helping us obtain ASC funding to help support the writing of this report.

Contents

List of Figures

Preface

Additive manufacturing (AM) techniques such as selective laser powder melting (SLM) hold great promise as the next big breakthrough in manufacturing. By building up a part step by step, using computer design and control, one could in principle attain very high precision and fidelity without having to compromise on the design for reasons of traditional manufacturing restrictions such as molding. In addition, it enables the production of replacement parts, remotely, and on demand, reducing the need for stocking large numbers of items. Because the part is build up small amounts of volume at a time, it is also feasible to embed specific small features ("barcodes") into the part that may not be visible form the outside, but allow for unambiguous identification. Similarly, it is conceivable that by tailoring the metal alloy one could modify or strengthen paretic in certain locations but not others. As the process is fully computer controlled such modifications and special features can be included without adding to the overall cost.

While AM is sometimes perceived as a brand new methodology, in reality its basic operation is about twenty years old. Initially it was known as rapid prototyping, highlighting one particular application: the ability to move quickly from shape to part without having to develop more involved production methods such as casting. Large manufacturers of aircraft engine parts, General Electric and Siemens (Germany) currently have actual active production plants based on AM techniques. For example, General Electric has committed to AM produce 40,000 valves for the Leap aircraft engine. Similarly, Siemens is also producing high value parts for engines. Neither company expects to see traditional manufacturing methods completely give way to AM, but both have made very significant investments it its development and application. Certainly, in the area of older aircraft there appears to be ample opportunity for AM, as there are large numbers of parts for which there are limited replacements. Here AM could play a valuable role by being able to quickly produce replicas of existing parts, using computer-aided design.

To fully realize the potential of SLM requires major advances in the areas of quality control and process control. A thorough understanding of the underlying physics of SLM and the development of robust and fast modeling tools are considered to be the key ingredients of a science-based program to support SLM. It is relatively straightforward to take a Computer-aided design (CAD) file of a particular object, say a wrench, and use Titanium powder particles to make a metal rendition of the wrench. It will have the shape and the dimensions specified in the CAD file. However, what is difficult is to predict the performance of the wrench. When and how will it break when put under stress is a question that is not straightforward to answer.

Experience has shown that the quality of the final part depends on a long list of materials properties (e.g., type of alloy, powder particle size) , as well as processing variables (laser beam power, scan rate, scan pattern, build direction). It is the goal of the industry, as expressed by the new government initiative America makes, the National Additive Manufacturing Innovation Institute, to facilitate the rapid development of modeling tools to enable the rational design of the

SLM process. Ultimately, and ideally, it would be advantageous to develop a virtual SLM machine, with which an engineer could test a design for a certain part, and discover how to optimize the SLM process to deliver a part that meets the specifications. From the manufacturing process settings, and associated materials properties on various length scales, the engineer is ultimately able to examine when and where the part will break under a certain load. Using those results, improved designs can be developed to optimize the parts design and manufacture. The latter two aspects, quite distinct in traditional manufacturing, will tend to merge somewhat in SLM because of the scale and the process underlying the additive manufacturing approach. A concept all too familiar in the world of living structures.

A crucial first step in the modeling of SLM is the prediction of voids and the development of a strategy to reduce their occurrence. Naturally, the presence of unintentional voids in the final part help to reduce the strength and the overall performance. To predict the void formation (and void size and location) one needs to have a realistic model of the basic dynamic wetting process that takes place when a small section of the powder melts, while in contact with surrounding powder and re-solidified metal surfaces. Void formation ultimately is a manifestation of a stochastic event feeding up information of local packing details of powder particles to the next larger length scale, the dimension of the melt pool. Thus, any realistic model will need to start at the point of melting, wetting and spreading of the melt pool. It should predict the developing melt pool and its final shape (and hence voids), and its connection with the rest of the powder bed, which will act as boundary conditions (for mass and thermal transport).

Only once the dynamic wetting and void formation problem problem is tackled is one in a position to consider more detail about the volume element that was converted from powder to a frozen melt pool in contact with its surroundings. For instance, from the thermal history of that melt pool (fast re-solidification) one could attempt to predict grain-size defect density and hence mechanical responses and ultimately possibly aging. However, it is not productive to focus on predicting detailed grain structure information, say, as long as one is unable to predict the presence, size and location of voids.

This page intentionally left blank.

Summary

The processes that underly the additive manufacturing technique known as selective laser melting include melting, re-solidification and and dynamic wetting of liquids. The latter is a process that, in general, operates on multiple length scales stretching from the molecular scale (e.g., contact line, surface reaction) to the mseoscopic (e.g., the powder particle level) to the macroscopic (e.g., an entire metal joint). In this report we focus on an aspect of dynamic wetting that greatly influences the additive manufacturing process, namely the formation of voids. Whereas an isolated collection of metal particles heated beyond the melting point would reliably form a single spherical liquid-metal drop, a similar collection surrounded by, and in touch with, solid powder particles as well as other proximate metal surfaces will adopt a shape and surface that might include voids. In both cases, the final shapes and contact areas are controlled by capillary forces, but the outcomes are quite different. The isolated collection that forms a single drop, has only one (liquid-vapor) interface, that is convex (i.e., spherical). In contrast, the environment of the other collection presents a complex surface to the molten metal, that can result in actively wicking of the droplet and a complex final shape.

Dynamic wetting is not an easy process to model on the meso scale (powder particle scale). That is because in additive manufacturing applications it takes place on a small scale set by the size of the particles that make up the metal alloy powder (of the order of 30-100μm), involves curved surfaces, surface roughness, compositional changes, and strong coupling to thermal processes (melting, conduction and re-solidification).

In this report we discuss the general problem of void formation and address the effect of compositional change on wetting in the context of thermodynamics and dynamics (i.e., Lucas-Washburn equation). Finally, we provide recommendations for the modeling of the selective laser melting technique, setting priorities for the different multiscale aspects of a comprehensive materials modeling program.

This page intentionally left blank.

Chapter 1

Introduction

In this paper we discuss the fundamental phenomena underlying selective laser melting of metal powders. The additive manufacturing (AM) process of selective laser powder melting is conceptually simple. It involves placing a powder sample and heating it with an energy source, such as a laser or an electron beam. The supplied heat will be sufficient to initiate melting of the powder particles. However, the melt pool will quickly solidify once the heat source has moved away from the volume element. This is so because the element is small (linear dimensions of about 100 microns) and is in contact with surrounding powder as well a previously solidified elements.

The goal of the manufacturing process is to convert a metal powder into a solid metal of a desired shape and size by repeatedly adding small amounts of material at a time. The challenge is to make the powder-solid conversion one of high fidelity: well adhered to surrounding solid, and free of entrapped voids. The latter are the number one difficulty faced in this type of AM, as voids become weak spots that initiate cracks and ultimately bring about failure of the part. The void fraction of a given manufactured part can in principle be determined by performing a density measurement, upon completion of the part. However, the objective is to avoid all void formation or, if they do occur, during the manufacturing process to spot them and treat them in situ.

The formation of voids is part of the capillary flow process that takes place when a small volume of the packed powder is rapidly converted into liquid. Because the surrounding powder presents as a porous material to the newly formed droplet, capillary phenomena dictate the flow of the droplet, the shape of the droplet and its contact area with its surroundings, and thus the possible formation of a void. At the outer surface of a part, the same physical processes will determine the surface finish of the part. It can be easily appreciated that since the powder placement will vary from location to location (as this is a reflection of the variability of the powder bed) that void formation, or the risk thereof, will continuously vary also. To improve the quality of parts, therefore, it will be key to learn how to reduce void formation and how to manage it if it does occur. Given the overwhelmingly large number of process variables (including: powder characteristics, laser scan rate, beam spot size, energy density) it is crucial that we develop a good understanding of the basic underlying phenomena (capillarity on a small scale), and that in the future we move toward a virtual manufacturing capability that assists the process engineer in the task of determining the optimal settings for the manufacturing process.

In turn, the contact area will determine how fast the droplet cools. This latter process will ultimately determine the grain structure, morphology and defect density of the re-solidified droplet.

This page intentionally left blank.

Chapter 2

Capillary Phenomena

Problem statement

The liquid drop that is formed once the heat source (e.g., the electron beam or laser beam) sufficiently heats the metal alloy powder, moves under the action of capillary forces. In general, in equilibrium, a liquid in contact with a solid surface will adopt a position and shape that corresponds to a configuration of lowest surface free energy (see figure 2.1). This includes the possibility of the liquid traveling, that is, its center of gravity may be undergoing translation. For instance, a liquid drop in contact with a capillary that is tapered, could move to the portion of the capillary that is most narrow.

The study of the equilibrium behavior of capillary fluids (i.e., capillary rise) has a a long history that goes back to the 18th century (Laplace) when experimentalists established the relationship between the contact angle and capillary rise, and contact angles and surface tensions (Young). In the early part of the twentieth century Lucas and, independently, Washburn considered the capillary driven flow inside capillaries. They established that the infiltration length is proportional to the square root of time elapsed.

In many contexts, including dynamic wetting in the SLM setting, an additional consideration appears and that is the role of reactive or dissolutive wetting. That is, wetting and spreading in the presence of changing interfacial composition. The effect on infiltration rate can be quite pronounced. In this chapter we consider capillary flow under circumstances of dissolution.

Introduction

The Lucas-Washburn equation describes the capillary driven flow into a pore or channel. It considers low Reynolds number laminar flow, or Hagen-Poiseuille flow, in a capillary and assumes that the pressure gradient is due to the capillary pressure difference across a curved surface.

The Washburn equation relates the infitration distance, L, and time, t, for capillary flow in a channel of diameter D, viz.,

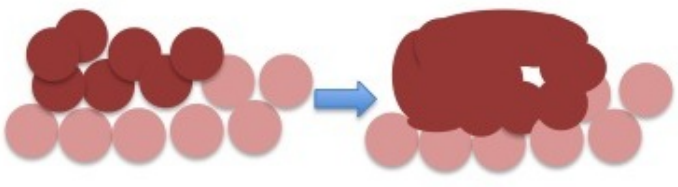

Figure 2.1. A schematic of the selective laser melting (SLM) process. A collection of powder particles are stacked on the left. A heat source (laser or electron beam) hits a sub set of the powder particles (indicated dark red). As these particular particles melt, in the presence of bystander particles (light red), the shape of the liquid droplet is determined by capillary flow (schematic on the right). In the example shown, a void is left that can persist, stabilized by surface energy considerations involving the bystander particles. This kind of void formation can compromise the performance of the final part.

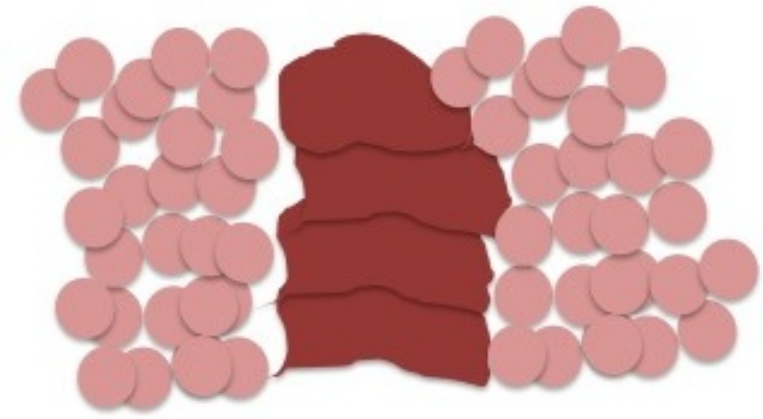

Figure 2.2. A schematic of the selective laser melting (SLM) process showing the build-up of a wall as a result of mulltiiple passes consisting of powder stacking and laser melting. As described in figure 2.1, capillary flow will determine the shape of each molten and re-solidified region. In the schematic shown, this is manifested in the surface finish of the part.

$$L^2 = \frac{D\gamma_{lv}cos\theta}{4\eta}t \tag{2.1}$$

where γ_{lv} is the liquid-vapor surface tension, θ is the contact angle and η is the viscosity.

Flow though cylinders.

We consider laminar flow through a circular cylinder with its axis along the $x-$direction. The Hagen-Poiseuille equation (which results from applying the no-slip boundary condition at the wall) links the velocity profile through a cylinder of radius R to the pressure differential Δp over the length of the liquid column L:

$$\begin{aligned} v_x &= -\frac{1}{4\eta}\frac{\partial p}{\partial x}(R^2 - r^2) \\ &= \frac{1}{4\eta}\frac{\Delta p}{L}(R^2 - r^2) \end{aligned} \tag{2.2}$$

from this expression we obtain the average velocity as

$$< v_x > \equiv (\pi R^2)^{-1} \int_0^R dr 2\pi r v_x = R^2 \Delta p / 8\eta L \tag{2.3}$$

For capillary flow into a cylinder the average velocity, $< v_x >$, represents the velocity of the meniscus, or the rate of change of the infiltration length. Hence

$$\frac{dL}{dt} = \frac{\Delta p R^2}{8\eta L} \tag{2.4}$$

or

$$LdL = \frac{\Delta p R^2}{8\eta} dt \tag{2.5}$$

which can be integrated from the initial time t_0 and the initial position L_0 to give,

$$L^2 - L_0^2 = \frac{\Delta p R^2}{4\eta}(t - t_0) \tag{2.6}$$

Specializing to a horizontal channel (no gravitational effects), a no-slip boundary condition and a pressure differential equal to the capillary pressure, we identify $\Delta p = 2\gamma_{lv} cos\theta / R$ [using the fact that the radius of curvature of a spherical meniscus equals $(1/R_y + 1/R_z)^{-1} = R/2$] :

$$L^2 = \frac{R\gamma_{lv} cos\theta}{2\eta}(t - t_0) + L_0^2 \tag{2.7}$$

which is, in essence, equation 2.1.

Flow through slits.

Next, we consider laminar flow between parallel plates, i.e., through a slit with the direction of flow along the $x-$direction. The Hagen-Poiseuille equation (which results from applying the no-slip boundary condition at the wall) links the velocity profile through a slit of diameter D to the pressure differential Δp over the length of the liquid column L:

$$\begin{aligned} v_x &= -\frac{1}{2\eta}\frac{\partial p}{\partial x}\left(\left(\frac{D}{2}\right)^2 - y^2\right) \\ &= \frac{1}{2\eta}\frac{\Delta p}{L}\left(\left(\frac{D}{2}\right)^2 - y^2\right) \end{aligned} \tag{2.8}$$

from this expression we obtain the average velocity as

$$< v_x > \equiv D^{-1}\int_{-D/2}^{D/2} dy\ v_x = D^2 \Delta p / 12\eta L \tag{2.9}$$

For capillary flow into a slit the average velocity, $< v_x >$, represents the velocity of the meniscus, or the rate of change of the infiltration length. Hence

$$\frac{dL}{dt} = \frac{\Delta p D^2}{12\eta L} \tag{2.10}$$

This can be integrated from the initial time t_0 and the initial position L_0 to give,

$$L^2 - L_0^2 = \frac{\Delta p D^2}{6\eta}(t - t_0) \tag{2.11}$$

Specializing to a horizontal channel (no gravitational effects), a no-slip boundary condition and a pressure differential equal to the capillary pressure, $\Delta p = 2\gamma_{lv} cos\theta / D$ [using the fact that the radius of curvature of a cylindrical meniscus equals $(1/R_y)^{-1} = D/2$] :

$$L^2 = \frac{D\gamma_{lv} cos\theta}{3\eta}(t - t_0) + L_0^2 \tag{2.12}$$

Testing the Washburn equation for nanosized channels.

To test equation 2.12 for capillary flow into molecularly sized slit-pores, Webb and Hoyt (WB)[3] performed molecular dynamics simulations of a Cu liquid flowing into a slit-like capillary made of Ni. Two types of simulations were run: nondissolutive (NDI) where the Ni atoms were not allowed to diffuse, and dissolutive (DI) where Ni atoms were fully dynamic and allowed to dissolve amongst the Cu (and vice versa). WB collected their simulation data in a graph of L^2 versus t (figure 6 of WB [3]), which shows that L^2 is linear with time for all four cases studied.

WB find that the slopes of the line are indeed close to best estimates of the coefficient $d\gamma cos\theta / 4\eta$. The exception is one case, labeled [d], for which the measured slope is about twice as large. WB proceed by proposing an additional driving force equation 2.6, leading to

$$L^2 = \frac{D\gamma_{lv} cos\theta + DQ_{diss}}{3\eta}(t - t_0) + L_0^2 \tag{2.13}$$

Invoking an additive driving force in the empirical manner of WB rationalizes an increased infiltration rate, but it is important to investigate its consequences. In particular, equation 2.13 predicts that capillary flow takes place even if the contact angle is greater than 90 degrees, i.e. negative $\cos\theta$, as long as $|\gamma_{lv} cos\theta| < Q_{diss}$, and this does not appear to be physical.

The justification for the additional term as well as its stated functional form, i.e., its dependence on D, is the focus of the remainder of this report. Below we will revisit the assumptions underlying the Washburn equation, investigate the implications of equation 2.13 and propose calculations or experiments that will be able to shed light on the situation.

The validity of equation 2.13.

Recall from the short derivation presented above, that it is the pressure difference $\Delta p = 2\gamma_{lv} cos\theta / D$ across the curved liquid-vapor interface that gives rise to the flow in a slit-like channel. by analogy, the WB suggestion amounts to introducing an additional pressure difference, i.e., $\Delta p_{diss} \equiv Q_{diss}/D$ into equation 2.2. In what follows we will explore the consequences of such a term in detail. To help clarify the subsequent discussion we will first highlight the basic physics and assumptions that underlie the Washburn equation.

The derivation of Washburn's equation starts with the the Navier-Stokes equation for an incompressible fluid,

$$(\vec{v}\cdot\nabla)\vec{v}+\frac{\partial\vec{v}}{\partial t}=\rho^{-1}\nabla p+\vec{g}+\eta\rho^{-1}\nabla^2\vec{v} \tag{2.14}$$

where ρ denotes the fluid density. Under the assumptions that 1) the flow is steady state, 2) the radial and swirl components are zero, and 3) absence of gravity, this equation simplifies to

$$\nabla p=\eta\nabla^2\vec{v} \tag{2.15}$$

For steady-steate flow through a straight cylinder, the velocity profile $\vec{v}=(v_x,0,0)$ is a function of r only, and the above version of the Navier-Stokes equation further reduces to:

$$\frac{\partial p}{\partial x}=\frac{1}{r}\frac{\partial}{\partial r}\left(r\frac{\partial v_x}{r}\right) \tag{2.16}$$

If one assumes no-slip boundary conditions at the wall the solution to this differential equation will be equation 2.2, or Hagen-Poiseuille flow.

As outlined in the section above, the Washburn equation results when the pressure difference, Δp, is equated with the Laplace pressure. The latter pressure is an equilibrium pressure (strictly: pressure difference) which can be measured directly. Specifically, in the presence of gravity, capillary rise will establish a pressure balance (hydrostatic equilibrium) between the Laplace pressure and the weight of a fluid column. This leads to a well-defined equilibrium height h for a given capillary size, liquid-vapor tension, and contact angle.

Let us now return to equation 2.13, in order to stay consistent with the physics underlying the Washburn equation, stipulating equation 2.13 forces one to identify the dissolution process with a pressure difference (or alternatively a pressure gradient, $\partial p_{diss}/\partial x$, since $\Delta p_{diss}=\int_{L_0}^{L}dx\ \partial p_{diss}/\partial x=-2Q_{diss}/D$). In addition, this pressure difference, Δp_{diss}, must represent an equilibrium quantity, and one would thus expect to be able to device an experiment to measure its magnitude. In the present context, it is natural to turn to a capillary rise experiment. Apparently, the prediction would be that in the presence of dissolution a nonzero Δp_{diss} exists that can be measured as a well-defined increase in h over the equivalent NDI capillary rise.

This argument can in fact be made more precise by reference to the Navier-Stokes equation. The key observation is that the Navier-Stokes equation of motion also embodies static equilibrium. That is, equation 2.14 reduces to

$$\nabla p=-\rho\vec{g} \tag{2.17}$$

In other words, just like capillary flow, the hydrostatic equilibrium of capillary rise is a manifestation of combining the Navier-Stokes equation with the Laplace pressure difference across a curved meniscus. Therefore, the prediction of an increased capillary rise in the presence of dissolution is based on the same footing as the prediction of equation 2.13 and, in addition, a capillary rise experiment could be used to measure Δp_{diss}. Since, by construction, this is an equilibrium experiment the measured rise must be solely determined by the final composition. The latter composition, strictly speaking, is determined by the chemical potentials, μ_{Cu} and μ_{Ni}. In other words, the final composition formally is the composition of the bulk system with which the pore is in actual or virtual equilibrium.

Alternatives to equation 2.13.

The arguments put forth above call into question the validity of equation 2.13 in its present form. Clearly, the simulations of WB establish that under dissolution conditions, and at a sufficiently high temperature , liquid Cu penetrates a Ni pore about twice as fast. It is pertinent therefore to consider other explanations for this observations that can do not suffer from the same criticisms.

Naturally, the first candidate for an alternative is to consider the effect of the dissolution process on the thermodynamic properties. As Ni dissolves into the Cu liquid changes are expected to occur in γ_{lv}, η and $cos\theta$ [1]. In principle, one could also consider changes in the temperature (due to the heat of mixing), the vapor pressure, and the liquid density. However, thermostatting keeps the temperature, T, constant, the metal vapor pressure is neglible at the temperature considered, while the liquid density (whose change is likely negligible also) does not enter the at level of the Washburn analysis (but is indirectly present through η).

With available data for $cos\theta$, but without presenting data for the composition dependence of γ_{lv} and η, WB do briefly discuss the possibility of thermodynamic property changes. The authors conclude that the changes would not be sufficient to explain the near doubling of the infiltration rate.

An alternative explanation for the increased infiltration can be pursued by focusing on the channel shape. Case [d] corresponds to NDI at a high temperature ($1750K$), and figure 1 of WB [3] [1] shows that a considerable amount of dissolution of Ni into Cu has taken place. In fact, that figure shows that the slit has tapered quite significantly opening up more toward the entrance. Since the picture shown is a projection, the actual tapering may even be more severe. It is, therefore, useful to consider the effects of tapering on channel flow.

[1] Figure 1 of WB [3] shows snapshots from MD simulations of liquid Cu infiltration into a Ni channel at T = 1750 K; results are shown for the non-dissolutive and the dissolutive simulations at varying simulation times: (a) t = 400 ps, (b) t = 900 ps and (c) t = 1400 ps.

Laminar flow in a slightly tapered cylindrical tube

Consider the case of no-slip and a tapered cylindrical channel. let the radius at the inlet be R_0 and at a distance L further downstream be R_L, that is

$$\frac{dR}{dx} = \frac{R_L - R_0}{L} \tag{2.18}$$

From equation 2.4 we have for the volumetric flow rate $Q = \pi R^2 < v_x >$:

$$Q = \frac{\pi \Delta p R^4}{8\eta L} \tag{2.19}$$

which we can rearrange to

$$\frac{dp}{dx} = -\frac{8\eta Q}{\pi R(x)^4} \tag{2.20}$$

where we replaced the pressure drop by its gradient $-dp/dx$ (see equation 2.2). Rearranging this we can write

$$\begin{aligned} dp &= -\frac{8\eta Q}{\pi R(x)^4} dx \\ &= -\frac{8\eta QL}{\pi (R_L - R_0)} R^{-4} dR \end{aligned} \tag{2.21}$$

where we used equation 2.18 to change variables from x to R. Upon integrating

$$\frac{p_0 - p_L}{L} = \frac{8\eta QL}{3\pi (R_L - R_0)} \left[R_0^{-3} - R_L^{-3} \right] \tag{2.22}$$

or in terms of the flow rate:

$$\begin{aligned} Q &= \frac{\pi \Delta p R_L^4}{8\eta L} \left[\frac{3\lambda^3}{1 + \lambda + \lambda^2} \right] \\ &= \frac{\pi \Delta p R_L^4}{8\eta L} f_C(\lambda) \end{aligned} \tag{2.23}$$

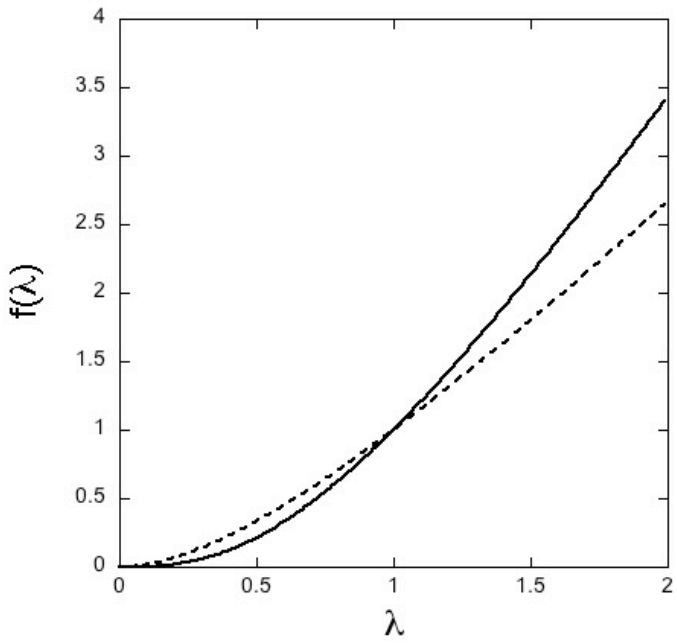

Figure 2.3. The tapering functions for cylindrical and slit-like geometry. The solid line denotes f_C (equation 2.23) while the dashed line represents f_S (equation 2.29) .

where $\lambda \equiv R_0/R_L$. The tapering effect is expressed by $f_C(\lambda)$ and, as expected, when $R_0 = R_L$ $f_C(\lambda) = 1$ and we recover the the straight channel result (cf. equation 2.3).

Laminar flow in a slightly tapered slit

The problem of flow through a slightly tapered slit-like channel of width w proceeds in an analogous fashion. Let the diameter at the inlet be D_0 and at a distance L further downstream be D_L, that is

$$\frac{dD}{dx} = \frac{D_L - D_0}{L} \tag{2.24}$$

From equation 2.10 we have for the volumetric flow rate $Q = wD < v_x >$:

$$Q = \frac{wD^3 \Delta p}{12\eta L} \tag{2.25}$$

which we can rearrange to

$$\frac{dp}{dx} = -\frac{12\eta Q}{wD(x)^3} \tag{2.26}$$

where we replaced the pressure drop by its gradient $-dp/dx$ (see equation 2.2). Rearranging this we can write

$$\begin{aligned} dp &= -\frac{12\eta Q}{wD(x)^3}dx \\ &= -\frac{12\eta QL}{w(D_L - D_0)}D^{-3}dD \end{aligned} \tag{2.27}$$

where we used equation 2.24 to change variables from x to D. Upon integrating

$$\frac{p_0 - p_L}{L} = \frac{12\eta QL}{2w(D_L - D_0)}\left[D_0^{-2} - D_L^{-2}\right] \tag{2.28}$$

or in terms of the flow rate:

$$\begin{aligned} Q &= \frac{\Delta p w D_L^3}{12\eta L}\left[\frac{2\lambda^2}{1+\lambda}\right] \\ &= \frac{\Delta p w D_L^3}{12\eta L} f_S(\lambda) \end{aligned} \tag{2.29}$$

where $\lambda \equiv D_0/D_L$. The tapering effect is expressed by $f_S(\lambda)$ and, as required, when $D_0 = D_L$ $f_S(\lambda) = 1$ and we recover the the straight channel result (cf. equation 2.10).

The two expressions, $f_C(\lambda)$ and $f_S(\lambda)$ are shown in figure 2.3. Notice that the deviation from linearity is stronger for the cylindrical case. This is to be expected, as the tapering in the slit affects only one dimension.

Now, returning figure 1(c) of WB [3] we note that the channel of the NDI case has become significantly tapered. An estimate for the ratio $\lambda = D_0/D_L$ gives about 1.3, and hence $f_S(1.3) = 1.47$. Thus, at the $t = 1400$ *ps* the volumetric flow rate would be expected to be larger by a factor of 1.5. This is likely a lower bound, as the projection used to produce figure 1(c) of WB [3] could mask a slightly larger tapering.

It is reasonable to conclude therefore that tapering could account for the increased rate of infiltration seen in the dissolution case, especially given the the uncertainties associated with the driving force, i.e. the combination $\gamma_{lv} cos\theta/\eta$.

Proposed work

In view of the analysis presented above a number of calculations suggest themselves. Restricting these to molecular dynamics (or Monte Carlo) the following would be worthwhile:

1. Using the WB geometry (and under NDI conditions) include a gravitational force, F_g, in the x-direction and perform an equilibrium simulation of capillary rise. Measuring the height, h, as a function of x_{Ni} (and possibly $|F_g|$) will yield a direct measurement of $\Delta p = \gamma_{lv} cos\theta/D$. This can be compared to the individual composition dependence of γ_{lv} and $cos\theta$. For details see Appendix

2. Repeat the above calculation under DI conditions. Some care must be taken to make sure that the capillary does not change its size, D, too much as Ni atoms dissolve into the Cu liquid. It would seem that the rise would have to be identical to that of a NDI simulation, provided the capillary size remains essentially unaffected.

3. Perform one or two WB capillary infiltration simulations for a Cu-Ni mixture at fixed x_{Ni} (i.e., using NDI conditions). This type of simulation has the attractive feature that it embodies all the composition dependence (i.e., of $\gamma_{lv}, cos\theta$ and η), without knowing the actual values. Need to specify the mass for Cu and Ni. To compare with reference [3], equal masses should be used.

4. Calculate γ_{lv} as a function of x_{Ni}, the Ni concentration, at $T = 1750K$ and possibly $T = 1500K$.

5. Calculate the equilibrium $cos\theta$ as a function of x_{Ni}. This is probably best done in a symmetric slit capillary, employing periodic boundary conditions in the $x-$ and $z-$directions. This will create two menisci that can each be used to extract the radius of curvature. In principle one could also use a sessile drop. In order to cover the relevant range of x_{Ni}, one should estimate the Ni composition in the flow simulation.

6. Calculate η as a function of x_{Ni}. This is probably best done with the Green-Kubo formalism, as it is guaranteed that the mixture will stay homogeneous and the molefraction known. Need to specify the mass for Cu and Ni.

7. Use the composition dependence of the $\gamma cos\theta/\eta$ factor to predict the infiltration rate as a function of x_{Ni}.

Appendix

Capillary Rise

The analysis of a capillary rise experiment starts with noting that the pressure in a horizontal plane (normal to the direction of gravity) must be the same everywhere. Thus, for a pure liquid column of height h the pressure difference Δp must equal $mgh(\rho_l - \rho_v)$ where, ρ_α denotes the number density of phase α and m is the atomic mass.

An exact treatment recognizes that the meniscus height z varies with position y. Formally, for every point (x,y) on the meniscus the local curvature must correspond to the local value $\Delta p = mgx(\rho_l - \rho_v)$. In practice, one would calculate Δp from a simulation as

$$\Delta p(y) = \frac{m < N(y) >}{\Delta y L_z} \tag{2.30}$$

Where $< N(y) >$ denotes the ensemble average of the number of atoms in a rectangular slice of width Δy, taking the size of the simulation box in the periodic $z-$direction as L_z. Note that we have assumed that the vapor pressure is essentially zero. Note also that this expression appears a little more direct since it avoids having to determine the local height x. This is so because the density $\rho_l(y) =< N(y) > /x\Delta y L_z$ also depends on the value of x. An other way of stating this is that the latter expression represents the self-consistent interpretation of ρ_l.

To improve statistics one would average equation 2.30 over the width of the capillary. This is equivalent to setting $\Delta y = D$.

The key observation is that a capillary rise (computer) experiment directly determines the term $\Delta p = 2\gamma_{lv} cos\theta / D$ which is the relevant combination determining capillary flow, or the Washburn equation. Its use is a matter of self-consitency that avoids the separate measurement of γ_{lv} and an ambiguous interpretation of $\cos\theta$.

Chapter 3

Nonequilibrium Surface Tensions

Introduction

In Chapter 2 we discussed the infiltration of liquid in a capillary, which for equilibrium liquids can be described quite well with the Lucas-Washburn equation. The infiltration length L was shown to be proportional to the square root of time, and the constant of proportionality was proportional to the product $\gamma_{lv}cos(\theta)$. The equation holds for equilibrium fluids, whether pure or mixed. In either case there exists a well-defined liquid-vapor surface tension, γ_{lv} and a well-defined contact angle, θ.

We then considered the situation of dissolutive wetting, where the solid boundary atoms dissolve into the liquid. The basic question we addressed was how does the Lucas-Washburn equation need to be modified? Computer experiments show that, in some cases, there is a factor of up to two increase when dissolution takes place.

Whereas Webb and Hoytt suggested the emergence of an additive term, we showed in Chapter 2 that this cannot be the correct functional form, as it would imply infiltration at zero contact angle, or even at negative contact angles if the WB dissolution term was sufficiently large. Instead, it would appear that the correct approach would involve an implicit dependence on time of both the tension and the contact angle, namely through:

$$\gamma_{lv}(\mathbf{x}(t)cos(\theta(\mathbf{x}(t)) \tag{3.1}$$

where $\mathbf{x}(t)$ denotes the composition of the liquid near the contact angle. This is time-dependent, since the dissolution is considered to continue to take place at the solid-liquid interface. Clearly at $t = 0$ when dissolution is considered to be starting, the product 3.1 is an equilibrium property of the liquid at the original equilibrium liquid composition. Similarly, for a drop sitting on a surface, at infinite times the product is that of the final equilibrium composition when equilibrium between the dissolving wall and the liquid has been reached. At that point the chemical potential gradients of all components vanish. Strictly speaking our notation should reflect the fact that the composition varies spatially, throughout the liquid. Formally, we should denote the composition by $\mathbf{x}(t,\mathbf{r})$, but we will assume in what follows that that is implied.

The question is what is the value for $\gamma_{lv}cos(\theta)$ at times in between, and how can we attempt to

predict it? Because the phenomenon we envisage is nonequilbrium in nature, there is 1) a priori no reason to assume that a simple answer exists for all cases, and 2) the expectation that the answer depends on the nature of the nonequilbrium situation. Thus, for a droplet in contact with a solid surface, the composition will change throughout the droplet, starting at the solid-liquid interface until the solubility product is reached and the composition becomes uniform. As this happens the contact area will change with time in response to changes in the product 3.1. The contact area may increase, decrease, or develop in a nonmonotonic fashion. On the other hand, for a capillary in contact with an infinite reservoir, the composition at the interface might reach at least a quasi-steady state as the meniscus continues to infiltrate the capillary, albeit with reduced speed.

Nonequilibrium Surface Tensions

To develop a description of dynamic wetting requires us to provide a theory to predict 3.1, or more simply put to predict the surface tension of an interface undergoing compositional changes. For ease of discussion we will concentrate on a surface that dissolves into the liquid, We will assume that the nature of the interface does not noticeably change in other ways, because the total amount of dissolution is small or because the dissolved atoms are replenished. This is a problem that has apparently not received much attention, since a paper by Ilan Aksay et al. in 1974. Which we will describe below.

A Brief Review of Surface Functions

Before we turn to the approach of Aksay et al.we briefly review surface functions. Consider a two-phase system, phase α coexisting with phase β. For convenience we assume that the two phases are separated by a planar interface thanks to a small gravitational field. It is possible to identify a specific surface contribution to thermodynamic functions such as the energy, U, and the Helmholtz free energy F. We assume that phases α and β occupy a volume V, and our first task is to assign a volume to each of the phases, that add up to the total volume,

$$V = V^{\alpha} + V^{\beta} \tag{3.2}$$

There is no unique way to do this. Instead, a choice has to be made as to the location of a mathematical plane that divides space between α and β. This plane has to be orthogonal to the surface normal, of the interface separating the two phases. That surface normal can always be unambiguously defined. However, the height of the dividing plane, the so-called Gibbs dividing plane, is arbitrary. This implies that the *value* of each of the surface functions we will introduce below will depend on the particular choice of dividing plane. Obviously, convenient choices are planes close to the visible interface.

Away from the the interface we can assign unambiguous intensive properties to each of the

phases, i.e., we can assign number densities, energy densities and free energy densities

$$\rho_i^\alpha = \delta n_i^\alpha / \delta V^\alpha \tag{3.3}$$
$$\phi^\alpha = \delta U^\alpha / \delta V^\alpha \tag{3.4}$$
$$\psi^\alpha = \delta F^\alpha / \delta V^\alpha \tag{3.5}$$

with similar quantities defined for phase β. The index i denotes a component (species). Finally, from the above we can define *extensive* properties for phases α and β, as

$$\mathbf{n}^\alpha = \rho^\alpha V^\alpha \tag{3.6}$$
$$U^\alpha = \phi^\alpha V^\alpha \tag{3.7}$$
$$F^\alpha = F^\alpha V^\alpha \tag{3.8}$$

In general, the sums like $\mathbf{n}^\alpha + \mathbf{n}^\beta$, $U^\alpha + U^\beta$, etc, are *not* equal to the totals of the actual two-phase system, $\mathbf{n}$, U etc, and it is precisely the the differences that define the surface contributions, $\mathbf{n}^s$, U^s etc. Thus,

$$\mathbf{n}^\alpha + \mathbf{n}^\beta + \mathbf{n}^s = \mathbf{n} \tag{3.9}$$
$$U^\alpha + U^\beta + U^s = U \tag{3.10}$$
$$F^\alpha + F^\beta + F^s = F \tag{3.11}$$

Note that the definition of surface functions does not rely on any particular interpretation of the interface (e.g., sharp or diffuse). It merely says there is one. Also, the values of the surface functions, because of the choice in dividing plane, are arbitrary, and so can have both positive and negative values. For one component systems, one often chooses the dividing plane location such that it makes $n^s = 0$. This is known as the *equimolar* surface. As soon as such a choice is made then all the values of the surface functions are fixed (i.e., U^s, F^s, etc).

If the two-phase system contains multiple components then one can no longer define a dividing plane for which all the n_i^s vanish. It is still possible to select an equimolar surface for a certain component i or, alternatively, one could decide to pick the plane for which the sum of all the products $\mu_i n_i^s$ adds up to zero. That is, $\mu \cdot \mathbf{n}^s = 0$.

The connection between F_s and the surface tension

The total free energy is homogeneous function of the volume V and the surface area A

$$F = -pV + \gamma A + \mu.\mathbf{n} \tag{3.12}$$

For the individual bulk phase α we have

$$F^{\alpha} = -pV^{\alpha} + \mu.\mathbf{n}^{\alpha} \tag{3.13}$$

and similarly for phase β. To obtain an expression for F^s, we subtract the bulk phase terms from equation 3.12. Thus,

$$F^s = \gamma A + \mu.\mathbf{n}^s \quad \text{or} \tag{3.14}$$
$$\gamma = F^s/A - \mu.\mathbf{n}^s \tag{3.15}$$

This establishes the connection between the surface tension and the so-called specific surface energy F^s/A. Whereas the surface tension is *independent* of the choice of dividing surface both terms on the right hand side of the equation are individually dependent on its location. We stress that it is only under the special conditions that the dividing surface is placed such that $\mu \cdot \mathbf{n}^s = 0$ that we have $F^s/A = \gamma$.

We define surface densities (sometimes referred to as excess densities) by dividing the surface quantities by A. For instance,

$$\Gamma_i = n_i/A \tag{3.16}$$
$$\phi^s = U^s/A \tag{3.17}$$
$$\psi^s = F^s/A \tag{3.18}$$

Γ_i is often referred to as the *adsorption* of species i. With this notion we can write:

$$\gamma = \psi^s - \sum_i \mu_i \Gamma_i \tag{3.19}$$

This is the notation used by Aksay et al.

The approach of Aksay et al.

Aksay et al. consider the effects of mass transfer of the kind we described (e.g. dissolution) at a solid liquid interface. Generically, they refer to this process as a chemical reaction, which is helpful in other ways as well. For the dissolution to occur, the total free energy, ΔG, must be decreasing. Aksay et al. then point out that the initial fee energy change of the the liquid is entirely attributable to changes in free energy in the interfacial region. Thus, they ad-hoc postulate that the decrease in specific interfacial free energy, $\psi^s = F^s/A$, is equal to the total change in free energy per unit area $\Delta G_{sl}/A$. They then quote equation 3.19 above,

$$\gamma = \psi^s - \sum_i \mu_i \Gamma_i$$

to relate the change in surface tension, $\Delta\gamma$, to $\Delta\psi^s$. Without explanation they simply equate the two. In other words, they ignore the contribution to the change of the last term of equation 3.20. Therefore the authors assume that $\Delta(\sum_i \mu_i\Gamma_i) = 0$.

Even if the dividing plane is located such that $\sum_i \mu_i\Gamma_i = 0$, that does not mean that the difference $\Delta(\sum_i \mu_i\Gamma_i)$ vanishes. Dissolution of the wall into the liquid increases the amount of one of the species (or adds an entirely new species), and this must make $\Delta(\sum_i \mu_i\Gamma_i) \neq 0$. Furthermore, equating $\Delta\gamma = \Delta\psi^s \approx \Delta G/A$ suggests that $\Delta\gamma < 0$, always. That is because a spontaneous process such as a surface reaction or dissolution always has $\Delta G \leq 0$. It is not difficult to use statistical mechanics to demonstrate that dissolution (or surface chemical reactions in general) could just as easily give rise to increases in the surface free energy.

A tractable example

To further explore the consequences of the Aksay ansatz we now focus on a simple thought experiment involving an isotope mixture. Consider an initially pure fluid A at a surface, and the solid surface dissolving an isotope B of that species into the liquid phase. Clearly, this dissolution process will produce a decrease in the free energy of the liquid, which will have no enthalpic contribution, and which is equal to an amount given by the ideal entropy of mixing. Yet, the surface tension of the pure fluids A and B and all their mixtures are the same, as the molecular interactions are all independent of the type of isotope (c.f., equation **??** below). In other words, we have $\Delta\gamma = 0$, and $\Delta\psi^s \approx \Delta G/A \neq 0$. Then by equation 3.20 we can conclude that $\Delta(\sum_i \mu_i\Gamma_i) \neq 0$. In fact, we must have $\Delta\psi^s = \Delta(\sum_i \mu_i\Gamma_i)$.

Next, we consider how to interpret the mixing term ΔG. Consider the dissolution of n^d wall atoms (species j, say) into the liquid phase, or $\Gamma^d = n^d/A$ atoms per unit area. To attribute an amount ΔG to this dissolution we can only proceed after we state the volume of liquid that the wall atoms dissolve into. In other words, it is only after we specify a profile for those atoms, or equivalently the equivalent thickness of the liquid layer (”slab”) that we can attempt to approximate the change ΔG. We assume we know the initial liquid composition, but to determine ΔG we must know the final composition of the thin slab, or the composition profile $x_j(z)$ for dissolving component j.

Statistical Mechanics

As is often the case with interfacial phenomena, turning to explicit problems and using the tried approaches of statistical mechanics can help elucidate the issues. In a previous report (SAND2013-8278) we have considered the case of an isomerization reaction at a planar wall, and shown how upon some further simplification (e.g., introducing the ideal solution assumption or the ideal gas assumption) one can formulate a tractable case that ultimately allows for the calculation of the surface tension as a function of time. That example mapped the problem of assigning a value to the nonequilibrium time-dependent surface tension $\gamma(t)$ onto the equilibrium surface tension illustration. We refer the interested reader to that report for more information.

This page intentionally left blank.

Chapter 4

Modeling of Additive Manufacturing Processes: Selective Laser Melting

Selective laser melting of powder beds is a process whereby a small amount of powder (10-1000 powder particles) are heated by laser, respond by melting, cool and ultimately resolidify.

The typical particle size distribution has an average diameter of 80μm and ranges from 45 - 115μm, and is assumed to be normally distributed. However, the employed average sizes can be as small as 50μm. The layer thickness employed varies, but typically falls in the range 50 - 200μm. The electron beam used has a maximum power of 3500 W, and a spot size of 100 - 400 μm.

Whereas an isolated cluster of such spheres would always form a spherical droplet, centered on the center of mass of the original cluster, a collection of powder particles in contact with surrounding particles (that do not melt), behaves quite differently. The collection of surrounding particles presents as a porous surface to the melt pool, and consequently we can expect capillary to dominate the flow of the droplet. After it has more or less come to rest, the shape of the pool and its connections with the surrounding surfaces.

Thus, it is the precise location of the powder particles that melt, together with the surrounding particles determine the final location and shape of the melt pool. This includes, therefore the occurrence of voids that are entrapped inside melt pools as well as between melt pools are their surrounding solid metal surfaces.

Given that a packing of 10 to 1000 particles is subject to large variations (no two piles are alike), SLM can be expected to exhibit large variations. It is precisely the stochastic nature of the process (i.e., the placement of powder particles) that translates in to variability upstream in the process. In particular, the occurrence of voids, the size and shapes of these voids is a direct reflection of the particulate nature of the starting material. Surface finish also is a different manifestation of exactly the same underlying physics.

The surrounding bed of powder particles acts in two ways on the emerging melt pool: 1) by inducing capillary flow, 2) through the liquid-solid interfaces it controls the heat flow out of the melt pool. The key observation is that these two aspects are *local* properties of the powder, and hence they ar subject to extreme variability. In contrast, the *global* thermal behavior of a large volume of the powder bed is a suitable spatial average over a large fraction of the granule

medium. As such it has a well-defined conductivity.

From the above It is clear therefore that any serious attempt at SLM modeling must start at the powder level. Any alternative homogeneous, continuum level approach will end up skipping over the essential physics, and cannot be expected to predict essential properties of the final resolidified metal part.

Once a proper model is employed for the melt pool one can consider further physical phenomena. An example is the evaporation of a Al, which has a low melting temperature and hence is more volatile than either Ti or V with which it is mixed in the alloy known as Ti-6Al-4V (or "Ti 6-4", this titanium alloy includes 6 w% aluminum and 4 w% vanadium, and less than 0.25 w% Fe and less than 0.2 w% O). From the diffusion coefficient of Al in Ti-6Al-4V, the total surface area (an possibly the curvature), and the thermal history one can estimate the final Al concentration inside the the melt pool. In addition, the concentration inside the powder particles will differ, because of size and manufacturing processes. Together, these effects produce a variation of the composition throughout the final AM part.

One expects that the spatial variation in composition will also be reflected in variations in the surface tensions and contact angles. The magnitude of the variation in (liquid-vapor) surface tension can be estimated from an equilibrium relationship between tension and molefraction. In the absence of this one could attempt to use modeling to determine the relationship.

Chapter 5

Conclusion

This report describes in detail what research and development is needed to use modeling to help support additive manufacturing and selective laser melting in particular. We have highlighted the issue of voids, which are inherent in the melting and resolidification of complex powder packings. However, we have also mentioned compositional variations due to preferential evaporation of Al. Modeling will enable a path forward in providing a science-based prediction of frequency of voids, their size and their location. At the heart of the modeling is the description of dynamic wetting in complex geometries. This phenomenon is further complicated by the presence of compositional variation in the melt pool, which affect the wetting and spreading. The report identifies and addresses the fundamental aspects of dynamic wetting in the context of additive manufacturing.

This page intentionally left blank.

References

[1] Note that it is the product of $\gamma_{lv} cos\theta = \gamma_{sv} - \gamma_{sl}$ that appears in the Washburn equation. Hence, formally one could look for the changes in the triplet γ_{sv}, γ_{sl} and η, but in practice this amounts to the same, given that a measurement of the solid surface free energies typically involves a contact angle.

[2] In principle, one could use $x = \Delta p / mg(\rho_l - \rho_v)$ to *define* the value of x, by assuming that the local densities ρ_l and ρ_v are constant, and can be measured well away from the meniscus. The advantage would be that more data contribute to the measurement of the local densities compared to a direct measurement of the local mensicus position x.

[3] E.B. Webb III and J.J. Hoyt *Molecular dynamics study of liquid metal infiltration during brazing*, Acta Materialia **56**, 1802 (2008)

DISTRIBUTION:

1	MS 0346	Mark F. Smith, 1830
1	MS 0828	Anthony S. Geller, 1516
1	MS 0836	Bradley Jarred, 1832
1	MS 0897	Ted D. Blacker, 1543
1	MS 1349	James E. Miller, 1815
1	MS 1349	William F. Hammetter, 1815
1	MS 1411	Amy Sun, 1814
1	MS 1411	Frank B. van Swol, 1814
1	MS 0899	Technical Library, 9536 (electronic copy)

Sandia National Laboratories